The following text is a preprint of the paper:
N. Fries, K. Odic, M. Conrath, M. Dreyer; The Effect of Evaporation on the Wicking of Liquids into a Metallic Weave; Journal of Colloid and Interface Science 321: 118-129, 2008.
www.elsevier.com/locate/jcis or
http://dx.doi.org/10.1016/j.jcis.2008.01.019

# The Effect of Evaporation on the Wicking of Liquids into a Metallic Weave

N. Fries, K. Odic, M. Conrath and M. Dreyer *

*Center of Applied Space Technology and Microgravity (ZARM), University of Bremen. Am Fallturm, 28359 Bremen, Germany*

**Abstract**

Wicking of liquids into porous media is of great importance to many applications. One example are propellant management devices (PMD) used in spacecraft tanks. PMDs are designed to ensure gas free delivery of propellant during all acceleration conditions of the flight. This might be achieved by a metallic weave which is wetted by the propellant and thus prevents gas from entering below a critical bubble point pressure. In the case of cryogenic or volatile liquids the weave may dry out and refilling of the structure becomes an important issue. In this study we analyze the wicking of different liquids into a dry Dutch Twilled Weave (DTW $200 \times 1400$) by combining experimental and analytical approaches. Experiments were performed under isothermal and terrestrial conditions to investigate the role of evaporation for the capillary rise. The standard wicking model from Lucas and Washburn is enhanced to account for evaporation and gravity effects, too. By comparing the experimental results with the enhanced wicking model we find good qualitative agreement. It is also noted that evaporation may have a major impact on the wicking process.

*Key words:* Capillary rise, Evaporation, Dutch Twilled Weave, Liquid penetration, Porous medium, Imbibition, Wicking, Lucas-Washburn equation, Washburn equation, heat pipe mesh

## INTRODUCTION

### *Motivation*

The main problem in spacecraft propellant tanks is the lack of gravity to define "up" and "down". Propellant management devices are designed to i) ensure a constant connection between propellant and tank outlet (communication type) or ii) confine the propellant at a designated location (control type) [1–3]. Fig. 1 shows a total communication type PMD including galleries with porous screen windows in them. The screens are made of a metal weave and are passive surface tension devices. They allow propellant to penetrate but prevent gas from entering below a critical bubble point pressure. This mechanism requires the weave to be always saturated with propellant. If the screen is partially dry, wicking can be regarded as a self healing mechanism to restore saturation. Hereby, wicking performance strongly depends on the degree of evaporation from the porous screen. This paper shows how fluid mechanic properties like the permeability of the weave are experimentally investigated, and presents a new evaporation model that allows to predict the effect of evaporation on the capillary rise.

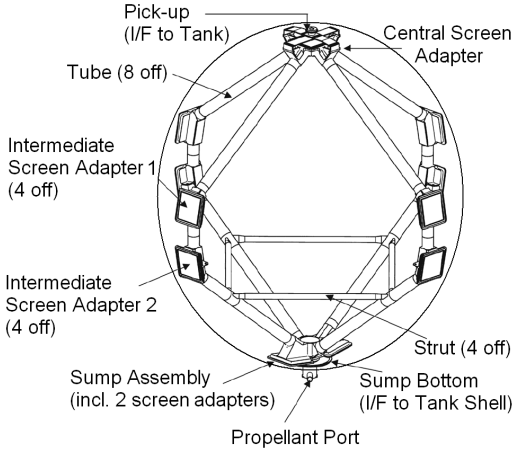


Fig. 1. Propellant management device (PMD) of the Automated Transfer Vehicle [4] (slightly modified).

### *State of the art*

When a fluid enters a porous medium due to capillary effects, a complex flow field develops within its pores. This

* Corresponding author.
E-mail address: dreyer@zarm.uni-bremen.de

wicking depends on geometrical and physical properties of both the weave (see Fig. 2) and the liquid. Many papers study this capillary penetration of liquids into porous media, some of them are summarized below.

Van Oss et al. [5] for example determine contact angles and pore sizes of porous media by column and thin layer wicking. They demonstrate that low-surface-energy liquids pre-wet the surface over which they subsequently spread. Siebold et al. [6] focus on total wetting liquids in powders for which contact angles are zero at equilibrium. They show that during the rising process the contact angle is higher than expected and propose a new method to calculate the constant terms in the Lucas-Washburn equation. A review article written by Bachmann et al. [7] describes the available methods to determine the wetting properties of porous media. Chibowski et al. [8] review existing literature on formulation and determination of free surface energy. Furthermore, they depict contact angle problems that also involve spreading liquids.

Theoretical studies of the wicking rate in porous media have also received significant attention. Many models of the pore space in such media are based on capillary tubes. This includes for example Lucas [9] and Washburn [10] who study dynamic invasion of fluid into a capillary, Levine et al. [11] who examine the departure from Poiseuille flow in the vicinity of an advancing meniscus in a vertical cylindrical capillary and Marmur [12] who examines the thermodynamic and kinetic effects on capillary penetration in systems of limited size. Symons [13] conducted a study to determine the magnitude of wicking rates in various screens including the one used in the present study: Dutch Twilled Weave (DTW) 200 × 1400. He developed an analytical model for the wicking process which expresses the wicking velocity as a function of liquid properties and geometrical parameters. His experimental data confirm the validity of his model. However, due to the complexity of the pore geometry within the screen it is necessary to merge several screen geometry parameters into a single constant. He also investigates the effect of evaporation and local heat sources. The extraction of pore structure parameters out of capillary rise observations is also described by Fries et al. [14]. Based on the momentum equation Stange [15,16] claims that the capillary rise process can be divided into four successive stages with i) an initial $h \sim t^2$ domain corresponding to the local acceleration of the liquid, ii) a $h \sim t$ domain related to the convective losses, iii) a $h \sim \sqrt{t}$ domain related to viscous dissipation and finally iv) a $h \sim 1 - e^{-(1+ct)}$ domain due to the gravity deceleration. The domains are separated by characteristic times.

The inertia dominated flow regime was also examined by Quere [17]. In the non-inertial capillary flow regime many authors, for example [2,13,10], favor a simple model in which the capillary pressure is balanced only by viscous friction and hydrostatic pressure. For many cases wicking in porous media can be regarded as a process where the inertial forces can be neglected most of the time.

## THEORETICAL MODEL (no evaporation)

When a liquid encounters a solid medium (as shown schematically in Figs. 4 and 5), a rapid rise of the liquid on the external surface occurs. This process is called wetting. If the solid medium has a porosity $\phi$ and a permeability $K$ there will be also an internal wicking beside the external wetting. Both processes rely on the capillary pressure, but in contrast to the wetting process the internal menisci that drive the wicking are bound to the pore radius $R_s$. The momentum balance for the wicking process gives

$$\frac{2\sigma\cos\theta_s}{R_s} = \frac{\phi}{K}\mu h v + \rho g h, \tag{1}$$

where $\sigma$ is the surface tension, $\theta_s$ the contact angle formed between solid and liquid, $\rho$ the fluid density, and $g$ gravity. The term on the left hand side represents the capillary pressure generated by the curvature of the liquid-vapor interface that is predetermined by the static radius $R_s$. This surface pressure is balanced by the terms on the right-hand side which correspond to viscous friction and gravity, respectively. The friction in Eq.(1) is expressed by Darcy's law (valid for laminar flow), which has also been used by Symons [13] and Marmur [18] in this context

$$\Delta p = \frac{\phi}{K}\mu h v, \tag{2}$$

where $\mu$ is the viscosity of the liquid, $v$ the (intersticial) velocity of the liquid and $h$ the fluid height in the medium. To extract the pore parameters $\phi$, $K$ and $R_s$ from measurements we use the approach that is proposed by Lucas [9] and Washburn [10]. By neglecting gravity and solving for the initial condition $h(t \to 0) = 0$ one obtains the Lucas-Washburn equation (here with permeability $K$)

$$h^2 = \frac{4\sigma\cos\theta_s}{\phi\mu}\frac{K}{R_s}t. \tag{3}$$

From this equation it can be seen that there is a linear correlation between $h^2$ and $t$ as long as the assumptions (no inertia, no gravity) hold. The maximum reachable height for $t \to \infty$ can be calculated. One obtains

$$h_{max} = \frac{2\sigma\cos\theta_s}{\rho g R_s}, \tag{4}$$

which is also used by Lucas [9] and others. The pore parameters of the material can now be calculated when $h(t)$ from the non-inertial, no gravity domain of the wicking process and $h_{max}$ from the final domain are known.

In their original equation Lucas and Washburn apply the Hagen-Poiseuille law used in the "bundle of capillary tubes" model

$$\Delta p = \frac{8\mu h v}{R_d^2}, \tag{5}$$

instead of Darcy's law that accounts for porous media. Here, $R_d$ is the mean hydrodynamic radius of the pores (Siebold et al. [6]). Comparing the Darcy and Hagen-Poiseuille law (Eqs. (2), (5)), one can directly relate the

permeability $K$ to the hydrodynamic radius $R_d$. Porosity $\phi$ is included as the two laws are defined for the interstitial velocity (Hagen-Poiseuille) and the superficial velocity (Darcy), respectively. Hence

$$\frac{8}{R_d^2} = \frac{\phi}{K}. \tag{6}$$

As mentioned before, Eq. (3) derived by Lucas and Washburn is only valid for flows with neither inertia nor gravity effects. Therefore, a fully analytic solution of Eq. (1) including gravity is given by Washburn [10] and Lukas and Soukupova [19] as well, however in terms of $t(h)$ and not $h(t)$. One may define two constants:

$$a = \frac{2\sigma \cos\theta_s}{\phi\mu} \frac{K}{R_s} \tag{7}$$

and

$$b = \frac{\rho g K}{\phi\mu}. \tag{8}$$

Using them in Eq. (1) and solving the resulting differential equation

$$\dot{h} = \frac{a}{h} - b \tag{9}$$

for the initial condition $h(t \to 0) = 0$ gives

$$t = -\frac{h}{b} - \frac{a}{b^2} \ln\left(1 - \frac{bh}{a}\right). \tag{10}$$

This equation allows to calculate the time $t$ needed for the wicking front to reach a certain height $h$. It can be transformed to a function $h(t)$ by mathematical means as shown by Fries and Dreyer [20].

To relate the imbibed fluid mass to the observed wicking height the following linear relation is assumed to hold

$$m = TW\phi\ \rho h, \tag{11}$$

with $W$ being the weave width and $T$ the thickness. Finally the Lucas-Washburn equation Eq. (3) can be modified to give the mass gain $m$ instead of the height $h$, resulting in

$$m^2 = (TW\phi\ \rho)^2 \frac{4\sigma \cos\theta_s}{\phi\mu} \frac{K}{R_s} t. \tag{12}$$

*Dimensional analysis*

To scale Eq. (1) it is appropriate to use the characteristic height $h_c = 2R_s$, a characteristic velocity

$$v_c = \sqrt{\frac{2\sigma}{\rho R_d}},$$

and a characteristic time

$$t_c = \frac{\rho R_d^2}{8\mu}.$$

This definition is, for example, used by Stange [15]. With the dimensionless variables $h^* = h/h_c$ and $v^* = v/v_c$ Eq. (1) reads

$$\cos\theta_s = 8\Lambda^2 \mathrm{Oh} h^* v^* + \mathrm{Bo} h^*. \tag{13}$$

Three dimensionless groups appear in this equation: an aspect ratio $\Lambda = R_s/R_d$, the Ohnesorge number

$$\mathrm{Oh} = \sqrt{\frac{2\mu^2}{\rho\sigma R_d}},$$

and the Bond number

$$\mathrm{Bo} = \frac{\rho g R_s^2}{\sigma}.$$

Using this scaling, the experimental results merge into one master curve, as shown later (see Fig. 9).

## EXPERIMENTS

*Weave and fluid properties*

Experiments were performed with a weave screen (see Figure 2) typical for the use within PMDs and test liquids with similar physical properties as typical propellants used in satellites (see Table 1). All liquids used in the experiments feature a near zero contact angle with respect to the weave material, but different vapor pressures which allows to investigate the effect of evaporation. As the static contact angle $\theta_s$ between all test liquids and the weave is near zero, $\cos\theta_s$ is assumed to be equal to one for all experiment evaluations.

Table 1
Fluid properties at 25 °C. Source: product data sheet of the listed liquids (3M for HFE 7500, FC-77, FC-72, FC-87 and Dow Corning for Silicone Fluid 0.65).

| | $\sigma$ | $\rho$ | $\mu$ | $p_v$ |
|---|---|---|---|---|
| | $10^{-3}$ | | $10^{-3}$ | $10^3$ |
| | [N/m] | [kg/m$^3$] | [Pas] | [Pa] |
| SF 0.65 | 15.9 | 758 | 0.49 | 4.4 |
| HFE-7500 | 16.2 | 1610 | 1.24 | 2.1 |
| FC-77 | 15.0 | 1780 | 1.28 | 5.6 |
| FC-72 | 12.0 | 1680 | 0.64 | 30.9 |
| FC-87 | 9.0 | 1650 | 0.45 | 81.1 |

The porous screen is a Dutch Twilled Weave (DTW) $200 \times 1400$ (Fig. 2 and Table 2). The samples are laser-cut in rectangular shapes with precise dimensions ($H = 50$ mm by $W = 10, 14, 16$ or 18 mm). They either have the warp wires or the weft wires running perpendicular to the screen width. If the wicking process is occurring parallel to the warp wires we define the flow to be in warp direction, correspondingly for the weft direction. The microstructure quality of each specimen is checked using a microscope to detect any defects at the edges of the samples. Subsequently, the selected weave undergoes a cleaning protocol that removes any dust or grease left on the surface or in the interstices. This is performed using an ultrasonic bath with a metal cleaner Turco (supplier: Henkel).

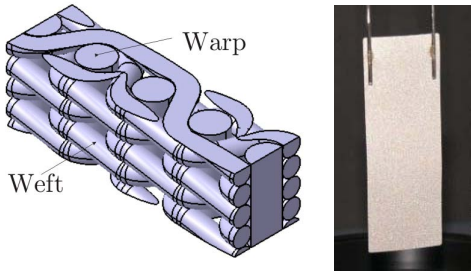


Fig. 2. Drawing of the microstructure (left) and photograph (right) of the Dutch-Twilled weave (DTW) 200 × 1400 (supplier: Spoerl).

Table 2
Properties of the weave.

| | |
|---|---|
| weave material | AISI 304 L (stainless steel) |
| type | Dutch Twilled Weave |
| 200 × 1400 | 200 warp wires/inch |
| | 1400 weft wires/inch |
| warp wire diameter [$\mu$m] | 70 |
| weft wire diameter [$\mu$m] | 40 |
| $H$: weave height [mm] | 50 ±0.01 |
| $T$: weave thickness [$\mu$m] | 149 ±1 |
| $W$: weave width [mm] | (10,14,16,18) ±0.01 |

*Experimental setup and data acquisition*

Fig. 3 displays an overview of the wicking experimental setup. Basically the setup consists of

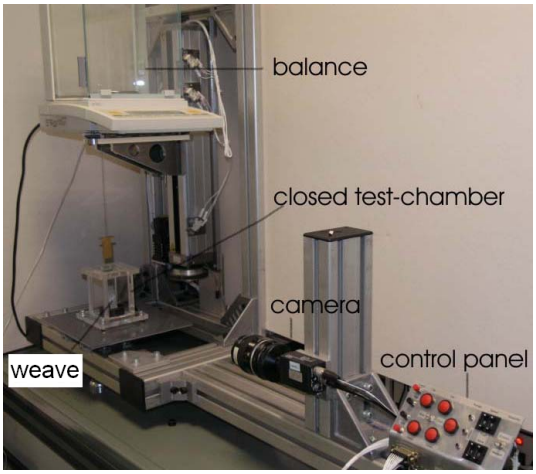


Fig. 3. Photography of the wicking experimental setup.

- a rectangular test chamber (50x50 mm$^2$ base area, 90 mm height) that contains the test liquid and the weave specimen suspended above the liquid surface,
- a video camera to record the wicking liquid front height versus time,
- an electronic balance with an accuracy of ±0.3 mg to which the weave is attached by threads.

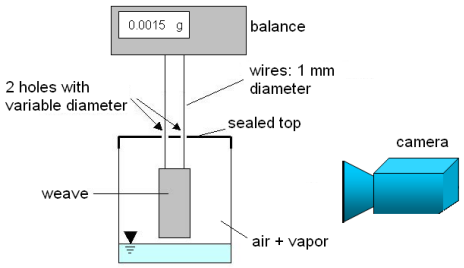


Fig. 4. Sketch of the test chamber prior to wicking experiments.

Fig. 4 shows a sketch of the arrangement. The weave is positioned for 1 hour above the test liquid surface prior to the experiment start. During this time no increase in the sample mass is recorded for all test liquids which means no significant capillary condensation occurs in the weave. The test chamber is closed, however there are two holes in the cover to attach the weave to the balance. Vapor diffusion through these holes can be adjusted as the size of the holes can be varied to investigate different evaporation rates. To further increase the evaporation rate the sealing top can be left open. The weave environment is therefore composed of air and vapor of the test liquid. The recording of the wicking front is done with a camera at 25 Hz. The resolution of the camera and the lens is 0.07 mm/pixel. The balance can be precisely and continuously moved up and down by means of an automated lift in order to sink the weave into the test liquid with a constant velocity of 1 mm/s. Data acquisition is controlled using the commercial software Labview.

The applied coordinate system is illustrated by Fig. 5 where the weave is immersed in the test liquid.

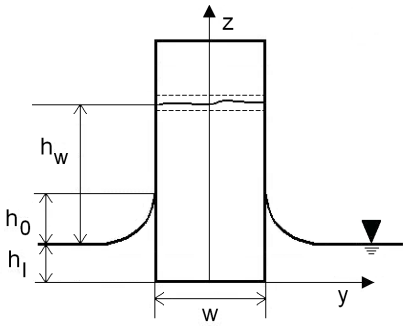


Fig. 5. Coordinates applied to the weave sample.

The height of the liquid front is the sum of three heights:

$$h = h_w + h_l + h_0. \tag{14}$$

Here, $h_w$ is the height due to the wicking process. $h_l$ is the immersion depth of the weave in the liquid, a safety length to ensure contact with the test liquid: $h_l \approx 0.55$ mm. $h_0$ is the height up to which the weave is covered with liquid due to the wetting phenomenon.

*Evaluation of experimental results - height approach*

By measuring the maximum achievable wicking height $h_{\max}$ that occurs due to the equilibrium between the capillary and the gravity forces (see Eq. (4)), the static radius $R_s$ can be calculated and thus, knowing $K/R_s$ from an other experiment, the permeability $K$. The maximum height is typically reached after about five days of liquid rise. In order to measure $h_{\max}$, an additional larger scale setup is used as $h_{\max}$ (depending on the liquid) is higher than the test chamber. The larger setup did not feature a balance but was sealed to prevent any evaporation. The results gave $R_s = (13.7 \pm 0.95)\ \mu$m.

Table 3
Maximum heights for $R_s = 13.7\ \mu$m and no evaporation.

| Fluid | SF 0.65 | HFE-7500 | FC-77 | FC-72 | FC-87 |
|---|---|---|---|---|---|
| $h_{max}$ [mm] | 312 | 150 | 125 | 106 | 81 |

To extract the permeability $K$ out of experimental results the linear part of $h^2(t)$ and $m^2(t)$ graphs can be used. In this domain of the wicking process the influence of gravity is negligible. Using Eq. (3) the parameter $K/R_s$ is extracted from the slope of the $h^2(t)$ curve.

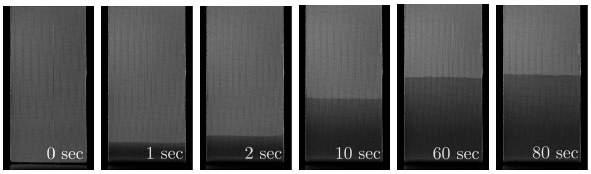


Fig. 6. Wicking of HFE-7500 into the weave.

An image series of the wicking process is presented in Fig. 6. The single frames of an image series are then processed with the commercial software MatLab to extract the actual wicking height. At the liquid front line, a mean height out of all pixel along the total width of the weave is calculated with a standard deviation of ±5 pixel as shown in Fig. 5.

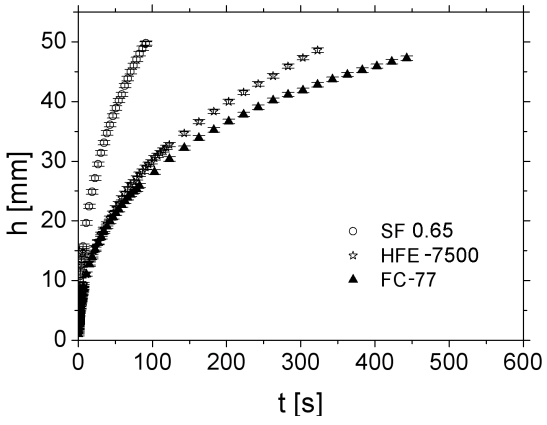


Fig. 7. Wicking height raw data (warp direction) with error bars (standard deviation is ±5 pixel).

Fig. 7 shows the resulting time dependencies of the wicking height for three test liquids and a 16 mm wide screen. As expected the slope is much steeper in the beginning of the measurement and decreases in time.

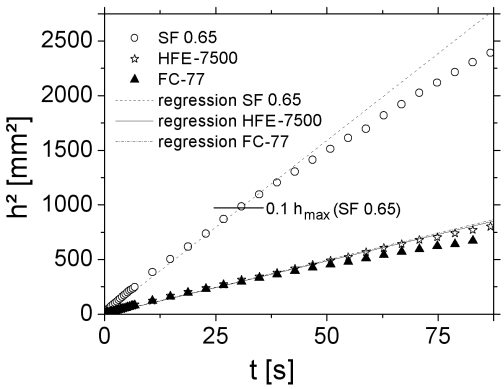


Fig. 8. Squared height over time (warp direction) with linear fitting (no error bars for graph clarity).

In Fig. 8, the squared height is plotted versus time. Near the origin a constant slope can be seen where a linear regression curve is calculated using the method of least squares to extract the pore parameters. For the linear regression the experimental values between the origin of the curve and $h$ up to about 10% of the maximum reachable height $h_{max}$ as given in Table 3 are used. This is consistent with the analytical solution presented by Fries and Dreyer [20] where under the influence of gravity the Lucas-Washburn equation is calculated to be valid for $h$ up to 10% of $h_{max}$. Table 4 contains the $K/R_s$ results for different fluids and their correlation coefficient.

Table 4
$K/R_s$ calculated from height measurements (warp direction). Numbers in brackets are correlation coefficients $r^2$, ± refers to the standard deviation. $K$ calculated with $R_s = 13.7\ \mu$m.

| | $K/R_s$ (experimental) [$\mu$m] | $K$ [$\mu$m$^2$] |
|---|---|---|
| SF 0.65 | 0.0589 (0.995) | 0.81 |
| HFE-7500 | 0.0448 (0.997) | 0.61 |
| FC-77 | 0.0506 (0.992) | 0.69 |
| Average | 0.0514 ±0.0071 | 0.70 ±0.10 |

The values from Table 4 reveal that there is a small deviation between the measurements made with different liquids. The average is $K/R_s = 0.0514\ \mu$m with a standard deviation of 0.0071 $\mu$m. Further measurements were also conducted using weaves with different widths ranging from 10 to 18 mm but a comparison of the results showed no significant influence of the width. The experimental data shown in Fig. 7 are now scaled with the characteristic numbers derived in the theoretical section, namely the Oh number and the Bo number. Fig. 9 shows the characteristic height scale versus the characteristic time scale for the experimental points and a numerical solution of Eq. (13). The

data collapses to one master curve. This confirms the relevance of the non-dimensional numbers to characterize the wicking behavior, but also enables the prediction of any other liquid front line height. The validity of numerical results applies approximately from $(t/t_c)$ Oh equal $3 \times 10^4$ to $1 \times 10^7$, while the lack of coincidence below $3 \times 10^4$ could be explained by the difficulty to get precise height respectively mass values at the beginning of the wicking process due the overlapping between wetting and wicking.

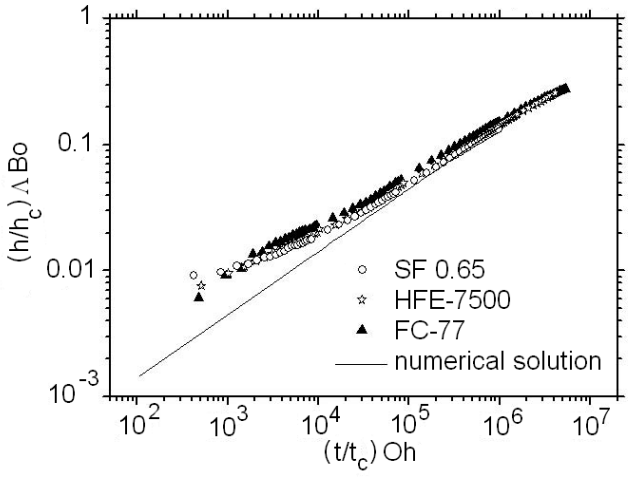


Fig. 9. Dimensionless representation of the experimental measurements (height method, warp direction) and numerical solution of Eq. (13) for the test liquids.

*Evaluation of experimental results - mass approach*

The chronology of a mass measurement is shown in Fig. 10. The curve is divided into six parts, describing the weave from the imbibition to the drying.

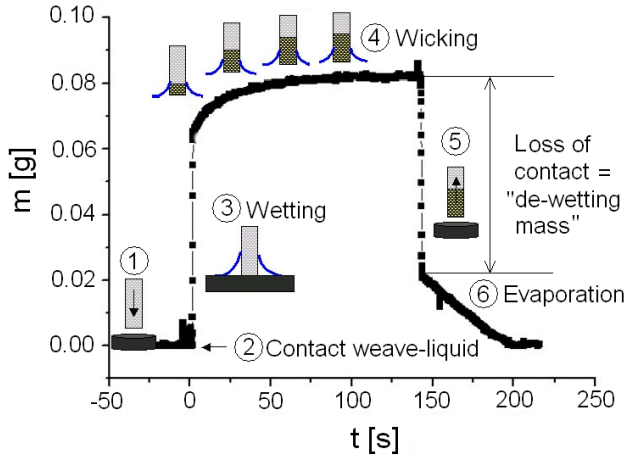


Fig. 10. Mass versus time curve (open test chamber). Imbibition of a weave (50x16mm) by HFE-7500.

At first, the weave is brought into contact with the test liquid inducing the wetting process. The liquid will then start to wick into the weave, while the mass will increase to finally reach a plateau value. In the absence of evaporation this corresponds to the equilibrium state between capillary and hydrostatic pressure. During the de-wetting the contact between weave and liquid is lost and the outer meniscus detaches. Finally, the last step belongs to liquid evaporation out of the weave which will only take place in unsaturated environments (e.g. open test chamber). This part of the curve is of great interest to evaluate the evaporation rate and will be described in further detail later. The result of a wicking mass versus wicking height measurement is shown in Fig. 11. It verifies the linear behavior and furthermore allows to calculate the "wicking effective porosity". Other methods to measure or predict the porosity of a weave are given by Armour and Cannon [21]. Using Eq. (11) the porosity can be calculated out of the slope (see Fig. 11) to be $\phi = 0.24 \pm 0.03$.

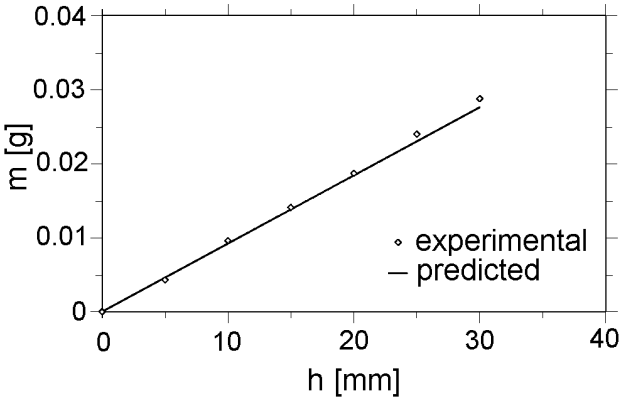


Fig. 11. Liquid mass inside the weave versus wicking height (HFE-7500 in 16 mm wide sample, warp direction). Prediction using Eq. (11).

According to Eq. (12) mass measurements can be used to calculate pore structure parameters like the permeability of the weave. The advantage of this "mass method" is that no image processing is necessary to evaluate the wicking height from video recordings. When considering experimental investigations using cryogenic liquids the mass method is an attractive alternative. This is because cryogenic liquids tend to render optical methods unpracticable by condensation on lenses. However, the mass method also features some disadvantages when compared to the optical measurement. As the weave is basically a two dimensional medium (0.15 mm thickness compared to 16 mm width) its wetted circumference is large compared to its volume. Thus the initial effect of wetting, the attachment of an outer meniscus to the weave, is a significant rise in mass when compared to the mass gain due to the wicking effect. As Fig. 10 illustrates, the wetting mass gain within a fraction of the first second is a significant portion of the total mass gain. Also, when the weave is brought into contact with the liquid, both effects occur at the same time and may be hard to distinguish. To obtain the "real wicking mass"

the "de-wetting mass" (see Fig. 10) is subtracted from the mass raw data, as the initial jump in mass refers to both the wetting and wicking process.

Analogous to the height method, Fig. 12 shows the squared wicking mass gain plotted versus time. From the

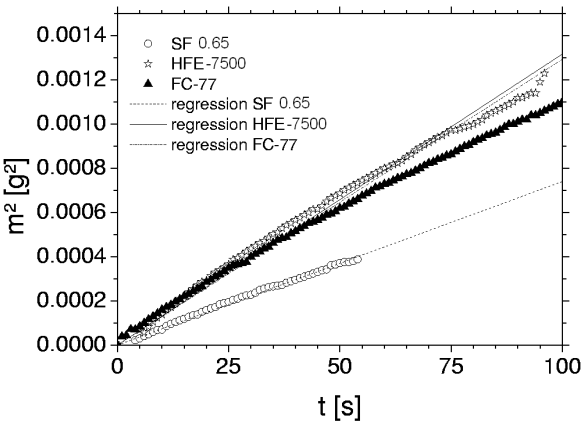


Fig. 12. Squared mass over time (warp direction) with linear fitting (no error bars for graph clarity).

slope of the $m^2(t)$ curves the weave parameters presented in Table 5 were calculated using Eq. (12). The values of Table 5 show good agreement with the ones calculated with the height method (Table 4).

Table 5
$K/R_s$ for the warp direction calculated from mass measurements. Numbers in brackets are correlation coefficients $r^2$, $\pm$ refers to the standard deviation. $K$ calculated with $R_s = 13.7$ $\mu$m.

| | $K/R_s$, warp [$\mu$m] | $K$, warp [$\mu$m$^2$] |
|---|---|---|
| SF 0.65 | 0.0565 (0.993) | 0.77 |
| HFE-7500 | 0.0544 (0.996) | 0.75 |
| FC-77 | 0.0496 (0.999) | 0.68 |
| Average | 0.0535 $\pm$0.0035 | 0.73 $\pm$0.05 |

The results presented in Table 6 refer to the capillary rise in weft direction. It is assumed that the static radius $R_s$ that defines the capillary pressure is equal for warp and weft direction. The mass and height curves for the weft direction are fairly similar to the ones in warp direction, however the liquid rises more slowly. This is due to the higher flow resistance in the weft direction. This can also be seen by the permeability $K$ in Table 6 which is about half the value of $K$ for the warp direction. An overview of our experimental findings is provided by Table 7. It also shows a comparison of the obtained results with literature which verifies our results to some extent. Dodge cites [22] as a source, where evaporation is not suppressed during the experiment. Thus, the higher evaporation rate may explain the deviation. Dodge does not use the pore parameters used in this work but his ones can be converted by the following correlations

$$\frac{\Phi_w}{D_{\mathrm{BP}}} = \frac{2}{R_s} \tag{15}$$

and

$$\frac{C_w}{B_s^2} = \frac{\phi}{K}. \tag{16}$$

Table 6
$K/R_s$ for the weft direction calculated from mass measurements. Numbers in brackets are correlation coefficients $r^2$, $\pm$ refers to the standard deviation. $K$ calculated with $R_s = 13.7$ $\mu$m.

| | $K/R_s$, weft [$\mu$m] | $K$, weft [$\mu$m$^2$] |
|---|---|---|
| SF 0.65 | 0.0255 (0.987) | 0.35 |
| HFE-7500 | 0.0283 (0.996) | 0.39 |
| FC-77 | 0.0259 (0.998) | 0.35 |
| Average | 0.0266 $\pm$0.0015 | 0.36 $\pm$0.02 |

Table 7
Overview - experimental results and comparison with literature (Dodge [23] and Symons [13]).

| | our value | Dodge | Symons |
|---|---|---|---|
| $\theta$: porosity | 0.24 $\pm$0.03 | | 0.272 |
| $R_s[\mu$m], warp | 13.7 $\pm$0.95 | 88.1 | 7.0 |
| $R_s[\mu$m], weft | 13.7 $\pm$0.95 | 124.4 | 7.0 |
| | our height method | Dodge | Symons |
| $K[\mu$m$^2]$, warp | 0.70 $\pm$0.10 | | |
| | our mass method | Dodge | Symons |
| $K[\mu$m$^2]$, warp | 0.73 $\pm$0.05 | | |
| $K[\mu$m$^2]$, weft | 0.36 $\pm$0.02 | | |
| $K/R_s[\mu$m], warp | 0.0535 | 0.0408 | 0.0462 |
| $K/R_s[\mu$m], weft | 0.0266 | 0.0132 | 0.0150 |

Dodge defines $\Phi$ as a screen characteristic parameter (not the porosity), $D_{\mathrm{BP}}$ as the effective pore diameter, $C_w$ as a wicking friction parameter and $B_s$ as the screen thickness. Symons uses a correlation constant $c$. For the static radius in warp direction Dodge obtains $R_s = 88.1$ $\mu$m and 124.4 $\mu$m for the weft direction. Symons uses $R_s = 7.0$ $\mu$m for warp and weft direction alike, however this value is based on the manufacturer's rated pore size. Altogether it can be seen that there is fair agreement between the $K/R_s$ values, however discrepancies for the $R_s$ results which may be explained by the sensitivity of the experiment to evaporation.

*The effect of evaporation*

Looking at Fig. 10, evaporation affects the periods 4 and 6. It is the only and hence crucial mechanism for the drying period 6, which is used for its measurement. It is characterized by the evaporation rate $\dot{m}_e$ which is the mass of evaporated liquid per area and time [kg/m$^2$ s]. $\dot{m}_e$ has to be calculated individually for each experiment as it depends on the used test liquid, temperature and saturation of the

surrounding air. To obtain different values of the evaporation rate the size of a ventilation hole on the top of the test chamber was varied. It could also be completely closed to prevent evaporation at all. Assuming evaporation from both sides of the weave the total mass flow due to evaporation is

$$\dot{M}_e = 2\dot{m}_e h(W+T). \tag{17}$$

Here, $h$ refers to the wetted height of the weave. The evaporation mass curves can roughly be divided into two drying periods. The first part of the curve is linear and corresponds to the drying when the weave is completely saturated. The second part which is nonlinear reveals a reduction of the drying rate when the amount of liquid is reduced below a certain level in the weave structure. As given by Kaviany [24], the liquid is trapped at this drying stage due to capillary forces. The effective evaporation rate which is of interest to understand the capillary rise under the effect of evaporation is the linear part, as it is assumed that the weave, once the wicking front has passed, is completely saturated and thus refers to this evaporation regime. As already mentioned by Symons [13], the wicking of a liquid into a weave can be effected by evaporation or local heat sources. In our study no external heat sources were applied. However, the experimental setup allowed to investigate the influence of different evaporation rates on the capillary rise in warp direction. The evaporation occurs due to the vapor pressure of the test liquids that leads to a layer of vapor over the weave surface. Due to diffusion and convection the vapor is distributed in the surrounding air so that more liquid can evaporate. It is assumed, since only relatively small amounts of liquid evaporate, that the enthalpy of evaporation can be neglected when compared to the heat capacity of the saturated weave and heat conduction from the gaseous species. As the weave is basically a two dimensional medium its outer surface is large compared to its volume which transports the liquid internally. Thus the effect of evaporation is fairly large. In Fig. 13 the different wicking heights of the test liquid HFE-7500 are presented. The influence of evaporation is clearly visible. The experiments were either performed by the authors or Kaya [25].

Table 8
Experiments performed using HFE-7500.

| | specimen width $W$ | chamber aperture | $\dot{m}_e$ (measured) |
|---|---|---|---|
| | [mm] | [mm$^2$] | [kg/m$^2$ s] |
| exp1 | 16 | 55 | $7.097 \times 10^{-6}$ |
| exp2 | 16 | 2500 | $4.357 \times 10^{-4}$ |
| exp3 | 18 | 55 | $1.808 \times 10^{-6}$ |
| exp4 | 18 | 2500 | $4.681 \times 10^{-4}$ |

Knowing about the strong effect of evaporation it is of interest to develop a model capable of explaining the process and allowing to predict the deviations from unaffected capillary rise.

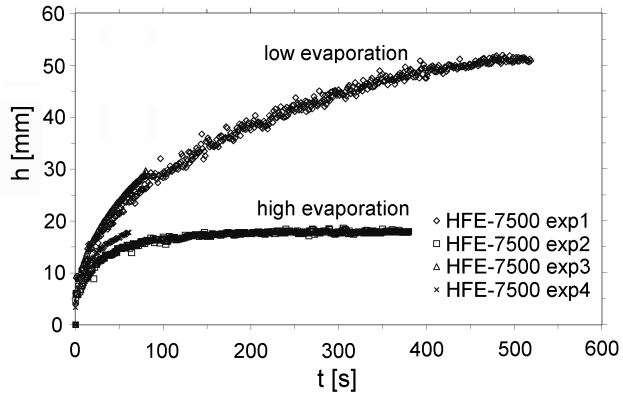


Fig. 13. Height calculated from mass recordings of HFE-7500 wicking into the weave. The evaporation rate affects the reached height significantly. See Table 8 for further details.

## EVAPORATION MODEL

While the liquid rises in the metal weave it is exposed to the ambient atmosphere at the outer pores. If the surrounding gas is not saturated with the vapor of the liquid, evaporation out of these pores can occur. Due to the continuous loss of liquid because of the evaporation the advance of the liquid front line will be more slowly than in a setup without evaporation. In this chapter we extend the theoretical model given by Symons [13], which can then be used to explain the experimental findings. For the model presented below the assumption has been made that the evaporation is uniformly distributed and is given by the area normalized evaporation rate $\dot{m}_e$ [kg/m$^2$ s]. The evaporation rate is constant $\dot{m}_e = const. \neq f(h,z)$. This assumption is valid if no point heat sources are affecting the local evaporation and if the transport of the gaseous (evaporated) species away from the weave is not restricted by the build up of a boundary layer (constant concentration gradient). Finally, the total evaporation mass flow $\dot{M}_e$ is given by Eq. (17) as stated in the previous chapter. Fig. 14 displays the integral and differential mass balance of the weave. It can be seen that the total mass inflow $\dot{M}(z=0)$ is made up of two components - the mass flow necessary to supply the movement of the liquid front $\dot{M}_{\dot{h}}$ and the total evaporation mass flow $\dot{M}_e$. $\dot{M}_{\dot{h}}$ is given by

$$\dot{M}_{\dot{h}} = \dot{h}\rho A_b = \dot{h}\rho W T \phi. \tag{18}$$

Here, $A_b$ refers to the effective bottom area of the weave. Regarding Fig. 14, the differential mass balance can be expressed as

$$d\dot{M}(z) = \dot{M}(z+dz) - \dot{M}(z) = -2\dot{m}_e(W+T)dz. \tag{19}$$

When integrating and using the boundary condition that the total mass inflow at $z=0$ must be equal to $\dot{M}_{\dot{h}} + \dot{M}_e$, one obtains

$$\dot{M}(z) = \dot{M}_{\dot{h}} + 2\dot{m}_e(W+T)h\left(1-\frac{z}{h}\right). \tag{20}$$

The local mass flow $\dot{M}(z)$ can now be given in form of a flow velocity which is then used to calculate the viscous

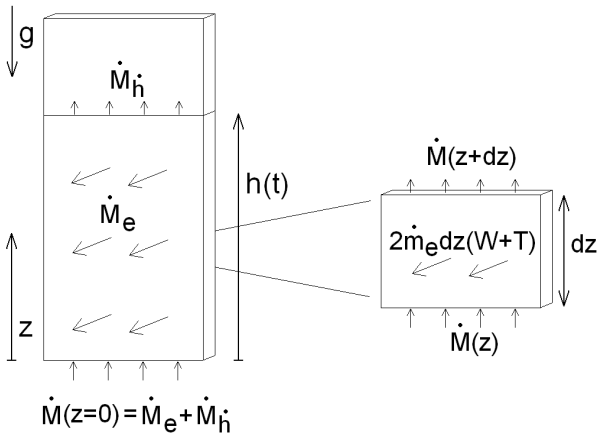


Fig. 14. Mass balance of a wicking process with evaporation.

pressure loss. The flow velocity in the weave is composed of two parts. The first part corresponds to the liquid front velocity $\dot{h}$, which is constant over the weave height as is $\dot{M}_{\dot{h}}$. The second is the refill velocity $v_r$ to refill the evaporated liquid, which is height dependent. Where the weave is in contact with the liquid surface ($z = 0$) the refill velocity reaches its maximum value of

$$v_{r,0} = \frac{\dot{M}_e}{\rho A_b} = \frac{2\dot{m}_e h(W+T)}{\rho WT\phi}. \tag{21}$$

The assumption of a constant evaporation rate at the outer weave surface leads to a linear dependence of the refill velocity (see Eq. (20)) reading

$$v_r(z) = v_{r,0}\left(1 - \frac{z}{h}\right), \tag{22}$$

thus it can be seen that $v_r$ linearly reduces to zero at the actual height $h(t)$. Fig. 15 displays the velocity distribution of the liquid inside the weave. The momentum balance of

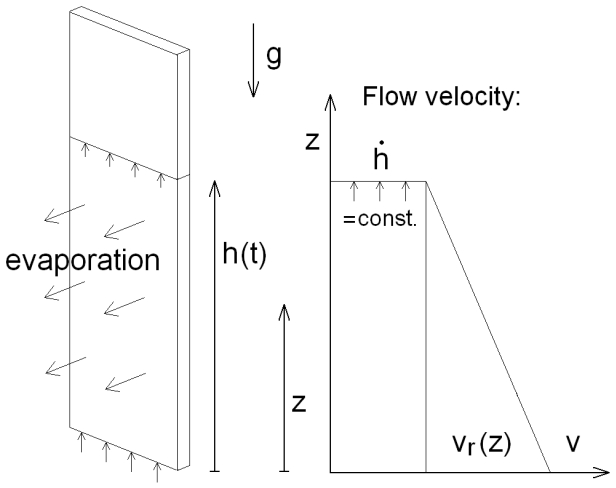


Fig. 15. Velocities involved in a wicking process with evaporation.

the liquid inside the metallic weave gives

$$p_c = p_h + p_{\dot{h}} + p_r \tag{23}$$

where the individual terms refer to (from left to right):
– capillary pressure ($2\sigma\cos\theta_s/R_s$)
– gravity term (hydrostatic pressure, $\rho gh$)
– viscous pressure loss $p_{\dot{h}}$ (Darcy) due to $\dot{h}$
– viscous pressure loss $p_r$ (Darcy) due to $v_r(z)$
The viscous pressure terms can be calculated as

$$p_{\dot{h}} = \frac{\phi}{K}\mu\int_0^h \dot{h}dz = \frac{\phi}{K}\mu h\dot{h}, \tag{24}$$

and with Eq. (22)

$$p_r = \frac{\phi}{K}\mu\int_0^h v_r(z)dz = \frac{\phi}{K}\mu\frac{1}{2}hv_{r,0}. \tag{25}$$

Thus, including the effect of evaporation, the final differential equation becomes

$$\frac{2\sigma\cos\theta_s}{R_s} = \rho gh + \frac{\phi}{K}\mu h\dot{h} + \frac{\mu\dot{m}_e(W+T)}{K\rho WT}h^2. \tag{26}$$

This equation can be transformed to the following form

$$\dot{h} = \frac{a}{h} - b - ch, \tag{27}$$

where the coefficients $a$, $b$ and $c$ are defined as

$$a = \frac{2\sigma\cos\theta_s}{\phi\mu}\frac{K}{R_s}, \tag{28}$$

$$b = \frac{\rho gK}{\phi\mu}, \tag{29}$$

$$c = \frac{\dot{m}_e(W+T)}{\rho WT\phi}. \tag{30}$$

Setting $\dot{h} = 0$ in Eq. (27) we find maximum heights for the following different cases: i) No evaporation occurs ($c = 0$) and only gravity restricts the maximum reachable height, given by

$$h_{max,a,b} = \frac{a}{b}. \tag{31}$$

ii) No gravity ($b = 0$) is affecting the liquid rise, however evaporation has an effect resulting in

$$h_{max,a,c} = \sqrt{\frac{a}{c}}. \tag{32}$$

iii) Both terms (gravity and evaporation) have to be considered leading to

$$h_{max,a,b,c} = \frac{-b}{2c} + \sqrt{\frac{b^2}{4c^2} + \frac{a}{c}}. \tag{33}$$

iv) Finally no gravity and no evaporation restrict the capillary rise, hence there is no limit in the maximum reachable height, as is also predicted by the Lucas-Washburn equation.

*Analytic solution*

Starting from Eq. (27) we can derive an analytic expression for the time needed to reach a certain height of the liquid front $t(h)$, accounting also for evaporation and gravity. Rewriting Eq. (27) gives

$$\int \frac{h}{-ch^2 - bh + a}dh = \int 1dt. \tag{34}$$

The solution to the first integral is given by Bronstein and Semendjajew [26] using the following definition

$$\Psi = -4ac - b^2. \tag{35}$$

For $\Psi < 0$ the total solution in terms of $t = t(h)$ is

$$t = \frac{-1}{2c} \ln\left(-ch^2 - bh + a\right) - \frac{b}{2c\sqrt{-\Psi}} \cdot \ln\left(\frac{-2ch - b - \sqrt{-\Psi}}{-2ch - b + \sqrt{-\Psi}}\right) + C. \tag{36}$$

To calculate the unknown constant $C$, the initial condition $h(t \to 0) = 0$ can be used to give

$$C = \frac{1}{2c} \ln(a) + \frac{b}{2c\sqrt{-\Psi}} \ln\left(\frac{-b - \sqrt{-\Psi}}{-b + \sqrt{-\Psi}}\right). \tag{37}$$

Thus the final solution is

$$t = \frac{1}{2c}\left[-\ln\left(\frac{-ch^2 - bh + a}{a}\right)\right] - \frac{b}{2c\sqrt{-\Psi}} \cdot \ln\left[\frac{(-2ch - b - \sqrt{-\Psi})(-b + \sqrt{-\Psi})}{(-2ch - b + \sqrt{-\Psi})(-b - \sqrt{-\Psi})}\right]. \tag{38}$$

*Dimensional analysis*

To compare the experimental data obtained with different fluids or under different conditions it is of great interest to have a set of dimensionless numbers to describe the problem. We introduce a dimensionless "capillary height number" HN relating gravity forces to surface tension forces and a "capillary time number" TN relating gravity forces to viscous and surface tension forces. These numbers are described in more detail by Fries and Dreyer [20]. The HN can be regarded as a special form of the Bond number since it relates gravity forces to surface tension forces, and is defined as

$$\mathrm{HN} = h\frac{b}{a} = \frac{hR_s\rho g}{2\sigma\cos\theta}, \tag{39}$$

where the TN is defined as

$$\mathrm{TN} = t\frac{b^2}{a} = \frac{tR_s\rho^2 g^2 K}{2\phi\sigma\mu\cos\theta} \mathrel{\widehat{=}} \frac{\mathrm{Bo}^2}{\mathrm{Ca}}. \tag{40}$$

Here the capillary number Ca relates viscous forces to surface tension forces and reads

$$\mathrm{Ca} = \frac{\mu v}{\sigma} \sim \frac{\mu R}{\sigma t}.$$

However, HN and TN are not able to reflect the influence of evaporation on the wicking behavior. This can be done by relating the maximum reachable height with gravity and evaporation (Eq. (33)) to the maximum reachable height without evaporation (Eq. (31)). Using this approach a dimensionless "related maximum height" $\Phi$ is obtained

$$\Phi = \frac{h_{max,a,b,c}}{h_{max,a,b}} = \frac{b}{a}\left(\frac{-b}{2c} + \sqrt{\frac{b^2}{4c^2} + \frac{a}{c}}\right). \tag{41}$$

If $\Phi$ is equal to zero no height is gained at all, the evaporation effect is so strong that it prevents any capillary rise ($\dot{m}_e \to \infty$). If $\Phi$ is equal to one, no evaporation occurs to restrict the capillary rise ($\dot{m}_e = 0$). For values of $\Phi$ in between, say 0.5, evaporation diminishes the reachable height to half the value that could be gained without evaporation. With these parameters we can draw a dimensionless plot of the numerical solutions of Eq. (26) as shown in Figs. 16 and 17. The numerical solution of Eq. (26) is consistent with the analytic one (Eq. (38)).

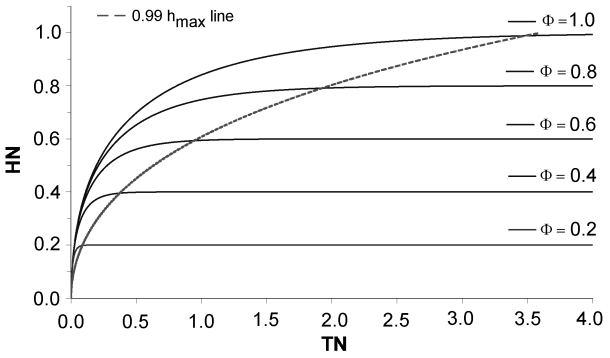


Fig. 16. Dimensionless height over time for different values of $\Phi$. 0.99 $h_{max}$ line is introduced in the next section.

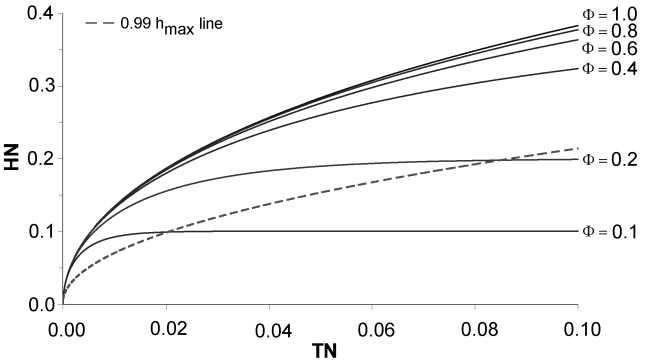


Fig. 17. Close up of the solution for shorter times.

*Time needed to reach 0.99 $h_{max}$*

For infinite times the gained height converges to a maximum value $h_{max}$. From Figs. 16 and 17 it can be seen that after a certain time depending on the evaporation rate, the height reaches a quasi steady state where no further increase in height occurs. For high evaporation rates (low values of $\Phi$) this state is reached earlier than for low evaporation rates (high values of $\Phi$). This raises the question at what time the liquid stops rising and reaches 0.99 times its maximum value $h_{max}$. Using numerical methods, namely a tool written in C++, the dimensionless time $\mathrm{TN}_{0.99}$ is found. It is defined as that time when 99% of the final height $h_{max}$ is reached. $\mathrm{TN}_{0.99}$ depends on the parameter $\Phi$ as can also be seen from the Figs. 16 and 17. A polynomial func-

tion of fourth order is fitted to the numerically generated points which gives

$$\mathrm{TN}_{0.99} = 1.2682\Phi^4 + 0.2157\Phi^3 + 2.122\Phi^2 - 0.0102\Phi. \quad (42)$$

The "0.99 $h_{max}$ line" in Figs. 16 and 17 refers to the inverted value $\Phi_{0.99}(\mathrm{TN}_{0.99})$ assuming that $\Phi$ is equal to HN when 99% of it is reached. Another interesting interpretation of the steady state line is as follows: If a liquid inside the weave is on the left hand side of the 0.99 $h_{max}$ line in the diagram, it is still rising. If it is on the right hand of the line, it has already reached its final height $h_{max}$ and remains static.

*Evaluation of the model with experimental data*

In this section the evaporation model introduced on the previous pages shall be compared to the experimental results obtained with the Dutch-Twilled-Weave 200x1400. The experiments were either performed by the authors or Kaya [25]. Figs. 18 and 19 show a comparison of experimental results and predicted values obtained with the presented model. Hereby the experiments are abbreviated by the liquid used and numbers as explained in Table 9.

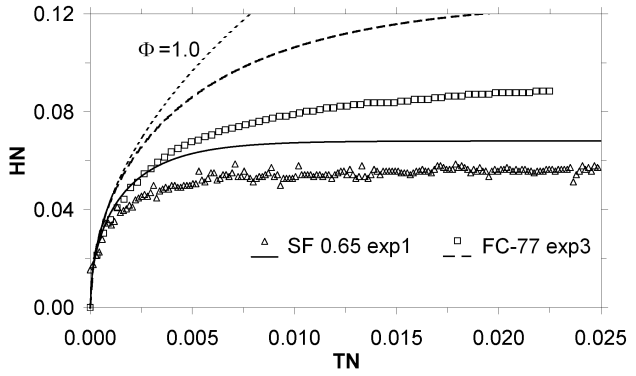


Fig. 18. A dimensionless plot (small TN) of experimental results (dots) in comparison to the values predicted by the model (lines). The $\Phi = 1$ line depicts the rise for both liquids with no evaporation.

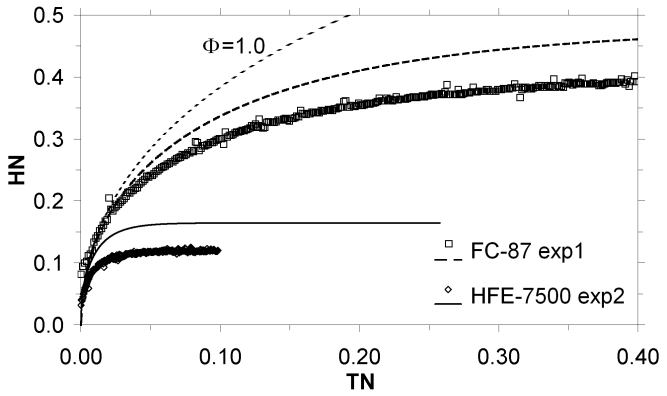


Fig. 19. A dimensionless plot (large TN) of experimental results (dots) compared to our model (lines).

From Figs. 18 and 19 it can be seen that in general the experimental results follow the predicted values. However,

Table 9
Experiments performed using various test liquids.

| | specimen width $W$ | chamber aperture | $\dot{m}_e$ (measured) | $\Phi_{calc.}$ |
|---|---|---|---|---|
| | [mm] | [mm$^2$] | [kg/m$^2$s] | [-] |
| HFE-7500 exp1 | 16 | 55 | $7.097 \times 10^{-6}$ | 0.740 |
| HFE-7500 exp2 | 16 | 2500 | $4.357 \times 10^{-4}$ | 0.169 |
| HFE-7500 exp3 | 18 | 55 | $1.808 \times 10^{-6}$ | 0.902 |
| HFE-7500 exp4 | 18 | 2500 | $4.681 \times 10^{-4}$ | 0.164 |
| FC-72 exp1 | 16 | 55 | $7.520 \times 10^{-5}$ | 0.529 |
| FC-87 exp1 | 16 | 55 | $1.657 \times 10^{-4}$ | 0.494 |
| FC-77 exp1 | 16 | 2500 | $2.006 \times 10^{-3}$ | 0.098 |
| FC-77 exp2 | 18 | 55 | $4.539 \times 10^{-6}$ | 0.847 |
| FC-77 exp3 | 18 | 2500 | $1.208 \times 10^{-3}$ | 0.124 |
| SF 0.65 exp1 | 16 | 2500 | $7.397 \times 10^{-4}$ | 0.071 |
| SF 0.65 exp2 | 18 | 55 | $4.680 \times 10^{-6}$ | 0.593 |
| SF 0.65 exp3 | 18 | 2500 | $6.576 \times 10^{-4}$ | 0.075 |

there seems to be a trend that the mathematical model overestimates the height. Table 10 displays the measured and predicted values of $\Phi$ to compare the deviation between model and experiment. Apparently the calculated values are larger than the measured ones as was seen from the comparison of the height curves. The average deviation is found to be in the range of 20%. There are several parameters which could be the source of these deviations. The contact angle is assumed to be constant which is not correct if the liquid interface is in motion. However comparison with models for the dynamic contact angle (e.g. Jiang et al. [27], based on data by Hoffman [28]) shows that the influence is negligible for the investigated flow regimes. For example using SF 0.65 fluid and a rise rate of 10 mm/s, which could only be reached within the first "fast" seconds of the process, one obtains a capillary number $\mathrm{Ca} = 3.1 \times 10^{-4}$ which leads to a $\cos(\theta)$ deviation of 3.4%. Another point is neglecting inertia effects which, however, should mainly be of importance for the very early stages of the capillary rise. Probably most influential is the assumption of a constant evaporation distribution all over the wet weave. If by some means the evaporation rate would be higher at the top of the weave the refill velocity $v_r(z)$ would not be a linear function of $z$ and thus more liquid would have to be transported to the top. This would lead to a higher pressure loss and may thus explain the discrepancy between theory and experimental findings. Despite the deviations the presented evaporation model gives a far better prediction for the capillary rise than solutions neglecting evaporation (e.g. Lucas-Washburn) and explains the experimental observations qualitatively. Also can be seen that realistic evaporation rates may have a major impact on the reachable wicking height. For example the last experiment shown in Table 10 (SF 0.65 exp1) has a measured $\Phi$ of about 0.06. This means the liquid reaches only 6% of the height that would be gained without evaporation!

Table 10
Experimental values of $\Phi$ compared to calculated ones.

| | $\Phi_{exp.}$ | $\Phi_{calc.}$ | $\Phi_{exp.}/\Phi_{calc.}$ |
|---|---|---|---|
| HFE-7500 exp2 | 0.12 | 0.169 | 71.0 % |
| FC-72 exp1 | 0.43 | 0.529 | 81.3 % |
| FC-87 exp1 | 0.40 | 0.494 | 80.9 % |
| FC-77 exp1 | 0.059 | 0.098 | 60.2 % |
| SF 0.65 exp1 | 0.057 | 0.071 | 80.3 % |
| average | - | - | 74.7 % |

## SUMMARY AND CONCLUSIONS

The wicking behavior of perfectly wetting liquids in metallic weaves is studied. By means of the momentum balance the Lucas-Washburn equation and further analytical solutions are introduced. An experimental setup using a vertically positioned weave is used to investigate the wicking behavior of different liquids. The results are compared to analytical solutions and good agreement between the Lucas-Washburn equation and the experimental data is found for flow regimes where gravity and evaporation effects are negligible. From the measurements characteristic pore parameters can be determined. No significant influence of the screen width is found on the wicking process. However, the capillary rise in warp direction occurs about twice as fast as in weft direction as the permeabilities also differ by about this factor due to the thicknesses of the wires and the weave structure. The results for the slope parameter $K/R_s$ are validated by previous literature, but there are discrepancies for the static radius which may occur due to the sensitivity of the experiment to evaporation. That is why the effect of evaporation is investigated in more detail and a model is developed to explain the observed effects. An analytical solution is presented which includes both gravitational and evaporation effects in dimensionless form. Using the introduced dimensionless parameters it is possible to plot all experimental data in a single diagram to compare different fluids and evaporation rates. The experimental data supports the theoretical model, although it shows that the model tends to overestimate the reached height by about 20%.

## ACKNOWLEDGEMENT

The funding of the research project by the German Federal Ministry of Economics and Technology (BMWi) through the German Aerospace Center (DLR) under grant number 50JR0011 and the Deutsche Forschungsgemeinschaft (DFG) through the Research Training Group PoreNet is gratefully acknowledged. The authors also like to acknowledge the support of Spoerl and the work of A. Kaya.

## References

[1] B.N. Antar and V.S. Nuotio-Antar. *Fundamentals of Low Gravity Fluid Dynamics and Heat Transfer*, chapter Chapter 9, pages 265–287. CRC Press, Boca Raton, Florida, 1993.

[2] F.T. Dodge. *Low-Gravity Fluid Dynamics and Transport Phenomena, editor J.N. Koster and R.L. Sani*, volume 130, chapter 1, pages 3–14. Aeronautics and Astronautics, Washington, DC, 1990.

[3] J.R. Rollins, R.K. Grove, and D.E. Jaekle. Twenty-three years of surface tension propellant management system design, development, manufacture, test, and operation. In AIAA, editor, *21st Joint Propulsion Conference*, pages 1–9. AIAA-85-1199, 1985.

[4] P.Behruzi, G.Netter. Concept analysis of PMD designs for future upper stages. *54th Int. Astronautical Congress, Bremen*, 2003.

[5] C. van Oss, R. Giese, Z. Li, K. Murphy, J. Norris, M. Chaudhury, and R. Good. Determination of contact angles and pores sizes of porous media by column and thin layer wicking. *J. Adhesion Sci. Technol.*, 6(4):413–428, 1992.

[6] A. Siebold, M. Nardin, J. Schultz, A. Walliser, and M. Oppliger. Effect of dynamic contact angle on capillary rise phenomena. *Colloids and Surfaces A*, 161(1):81–87, 2000.

[7] J. Bachmann, S.K. Woche, M.O. Goebel, M.B. Kirkham, and R. Horton. Extended methodology for determining wetting properties of porous media. *Water Resour. Res.*, 39(12), 2003.

[8] E. Chibowski and R. Perea-Carpio. Problems of contact angle and solid surface free energy determination. *Advances in colloid and interface science*, 98:245–264, 2002.

[9] R. Lucas. Ueber das Zeitgesetz des kapillaren Aufstiegs von Flüssigkeiten. *Kolloid-Zeitschrift*, 23:15–22, 1918.

[10] E.W. Washburn. The dynamics of capillary flow. *Physical Review*, 17(3):273–283, 1921.

[11] S. Levine, J. Lowndes, E.J. Watson, and G. Neale. A theory of capillary rise of a liquid in a vertical cylindrical tube and in a parallel-plate channel. *J. Colloid Interf. Sci.*, 73(1):136–151, 1980.

[12] A. Marmur. Penetration and displacement in capillary systems of limited size. *Adv. Colloid Interfac.*, 39:13–33, 1992.

[13] E.P. Symons. Wicking of liquids in screens. *NASA TN D-7657*, 1974.

[14] N. Fries, K. Odic, and M. Dreyer. Wicking of perfectly wetting liquids into a metallic mesh. *Proceedings of the 2nd International Conference on Porous Media and its Applications in Science and Engineering; Kauai, USA*, 2007.

[15] M.Stange, M.Dreyer, H.Rath. Capillary driven flow in circular cylindrical tubes. *Phys. Fluids*, 15(9):2587–2601, 2003.

[16] M. Stange. *Dynamik von Kapillarströmungen in Zylindrischen Rohren.* Cuvillier, Göttingen, 2004.

[17] D. Quere. Inertial capillarity. *Europhys. Lett.*, 39(5):533–538, 1997.

[18] A. Marmur. Kinetics of Penetration into Uniform Porous Media: Testing the Equivalent-Capillary Concept. *Langmuir*, 19:5956–5959, 2003.

[19] D. Lukas and V. Soukupova. Recent studies of fibrous materials wetting dynamics. *In INDEX 99 Congress, Geneva, Switzerland*, 1999.

[20] N. Fries and M. Dreyer. An analytic solution of capillary rise restrained by gravity. *J. Colloid Interf. Sci.*, 320:259–263, 2008.

[21] J.C. Armour and J.N. Cannon. Fluid flow through woven screens. *AIChE Journal*, 14(3):415–420, 1968.

[22] F.T. Dodge and E.B. Bowles. Vapor flow into a capillary propellant-acquisition device. *19th Joint Propulsion Conference, Seattle, Washington, AIAA-83-1380*, 1983.

[23] F.T. Dodge. *The New Dynamic Behavior of Liquids in Moving Containers.* Southwest Research Institute, San Antonio, Texas, 2000.

[24] M. Kaviany. *Principles of Heat Transfer in Porous Media*. Springer, New York, 1995.

[25] A. Kaya. Untersuchung des Eindringverhaltens von Flüssigkeiten in poröse Medien. *Thesis (Diplomarbeit), University of Bremen*, 2007.

[26] I.N. Bronstein and K.A. Semendjajew. *Taschenbuch der Mathematik*. Teubner, 1985.

[27] T.-S. Jiang, S.-G. Oh, J.C. Slattery. Correlation for dynamic contact angle. *J. Colloid Interf. Sci.*, 69:74–77, 1979.

[28] R.L. Hoffman. A study of the advancing interface. I. Interface shape in liquid-gas systems. *J. Colloid Interface Sci.*, 50:228–241, 1975.